Journal of Industrial Intelligence
https://www.acadlore.com/journals/JII

A Characterization Model for Vibration Hazards in Mining Equipment Based on Time-Frequency Mask and Sparse Representation

Yunbo Li[1*], Hongling Peng[2]

[1] School of Electronic and Information Engineering, Guang'an Vocational and Technical College, 638000 Guangan, China
[2] Detection Branch Institute, China Coal Science and Engineering Group Chongqing Research Institute Co., Ltd, 400037 Chongqing, China

* Correspondence: Yunbo Li (40666345@qq.com)

Received: 11-20-2024 **Revised:** 12-21-2024 **Accepted:** 12-26-2024

Citation: Y. B. Li, H. L. Peng, "A characterization model for vibration hazards in mining equipment based on time-frequency mask and sparse representation," *J. Ind Intell.*, vol. 2, no. 4, pp. 212–217, 2024. https://doi.org/10.56578/jii020402.

Abstract: A wide range of safety hazards exist in underground coal mines, characterized by unpredictability, randomness, and coupling effects. The increasing structural complexity and diversity of underground equipment present new challenges for fault state monitoring and diagnosis. To address the unique characteristics of underground equipment fault diagnosis, a characterization model of vibration hazards was proposed, integrating a time-frequency mask-based non-stationary filtering technique and sparse representation. Experimental analysis demonstrates that the time-frequency mask algorithm effectively filters out sharp non-stationary noise, restoring the original stationary healthy signal. Compared to Support Vector Machine (SVM), Convolutional Neural Network (CNN), and Principal Component Analysis (PCA), the sparse representation algorithm exhibits superior performance in characterizing vibration hazards, achieving the highest accuracy.

Keywords: Vibration hazards in equipment; Time-frequency mask and sparse representation; Vibration hazard characterization

1 Introduction

Coal remains a fundamental resource and a primary energy source in China, playing a critical role in ensuring national economic development. Over the long term, coal is expected to remain the dominant energy source. Currently, coal accounts for approximately 56% of China's primary energy consumption, contributing to three-fourths of the total domestic energy production. Projections indicate that coal will constitute 50% of China's energy consumption by 2030 and approximately 35% by 2050. Compared to major coal-producing countries such as the United States, Australia, and India, China's coal reserves are buried at greater depths and are associated with more complex geological conditions. Various mining hazards, including gas outbursts, water inrush, dust accumulation, and spontaneous combustion, often coexist in underground coal mines. Additionally, over 95% of coal mining operations in China rely on underground mining techniques, whereas in the United States, Australia, and India, underground mining accounts for less than half of total coal production.

Underground mining involves multiple production processes, including extraction, tunneling, transportation, and ventilation, which form highly complex systems and significantly increase the difficulty of monitoring and supervision. Numerous safety hazards exist in underground coal mines, characterized by unpredictability, randomness, and coupling effects, all of which pose risks of severe accidents that threaten mine safety. These hazards encompass unsafe human behaviors, hazardous conditions of equipment and materials, and environmental risks. Traditional manual monitoring methods suffer from limitations in hazard identification, such as inadequate recognition capabilities and unmonitored areas, making it challenging to detect and eliminate risks promptly. In recent years, artificial intelligence (AI) technologies have increasingly been applied to the identification of underground safety hazards in coal mines. Some enterprises have achieved notable breakthroughs, enabling field trials in specific scenarios. However, due to the highly specialized and complex mining environment, large-scale deployment of such technologies remains unfeasible. With rapid advancements in science and technology, coal mining equipment has

become increasingly integrated, high-speed, and intelligent. Consequently, the structural complexity and diversity of equipment have intensified the challenges associated with monitoring and diagnosing equipment faults. Acoustic diagnosis techniques have gained prominence in this domain due to their unique advantages and have emerged as a key research focus in fault detection and monitoring [1–12].

Over the past several decades, vibration-based fault diagnosis technology has developed into a well-established and comprehensive system, generating substantial economic benefits. The United States holds a leading position in this field, with companies such as Bently and HP producing monitoring systems that represent the state-of-the-art in fault diagnosis technology. These advanced monitoring systems have been widely applied in aerospace, military, chemical, and other industries. In China, research on mechanical fault diagnosis began in the late 1970s and early 1980s. Although development commenced later than in the United States, significant progress has been made in both theoretical research and technological applications. Several key research institutions in China have developed practical diagnostic systems. For instance, the BH5000 series diagnostic system, developed by the Chemical Safety Engineering Center at Beijing University of Chemical Technology, has been successfully commercialized in the chemical industry, leading to the establishment of Beijing Bohua Xinzhi Technology Inc., which specializes in condition monitoring, fault diagnosis, and intelligent maintenance of large-scale equipment and has achieved significant economic and social benefits. Similarly, Chongqing University utilized the CDMS system to conduct tests and fault diagnosis on fans at the Yushan Mineral Processing Plant of Yunnan Tin Industry Company, successfully detecting eight cases of bearing faults. Currently, the diagnosis of faults in underground mining electromechanical equipment primarily relies on vibration signal monitoring. However, this approach depends heavily on experienced field professionals with expertise in signal analysis to ensure accurate fault identification. The shortage of skilled personnel in mining enterprises has hindered the widespread adoption of vibration-based fault diagnosis methods. With the advancement of machine learning technologies and their application in coal mines, the use of audio signals for identifying potential hazards in underground mining electromechanical equipment has become an emerging research focus [13–22].

2 Non-Stationary Noise Filtering Technique Based on Time-Frequency Mask

The short-time Fourier transform (STFT) obtains a series of frequency spectra that vary over time, thereby capturing the time-frequency characteristics of a signal. These time-frequency characteristics effectively describe the frequency distribution within a given time segment, providing valuable information for subsequent signal processing. Given a signal x, its STFT can be represented as a matrix X. The power spectral matrix W is obtained by squaring the elements of X:

$$W(i,j) = X(i,j)^2 \tag{1}$$

where, $i = 1, 2, \ldots, K$ denotes the number of rows in X, corresponding to the number of frequency bands in the STFT spectrum, $j = 1, 2, \ldots, M$ represents the number of time windows in the STFT, and W is the power spectrum.

The power spectral matrix characterizes the temporal variations of power at certain frequencies, which exhibit periodic fluctuations in response to the periodicity of the signal. By computing the autocorrelation coefficients of each row in the power spectral matrix, the periodic variation of power in each frequency band over time can be analyzed.

$$A(i,j) = \sum_{j=1}^{n-h} \frac{W_{i,j} W_{i,j+h}}{\sum_{j=1}^{n} {W_{i,j}}^2} \tag{2}$$

Let A denotes the autocorrelation function matrix and j the order of the autocorrelation. By summing the autocorrelation coefficients across all frequency bands, the overall variation of the signal's autocorrelation coefficients over time can be obtained:

$$SA(j) = \sum_{i=1}^{k} A(i,j) \tag{3}$$

where, SA represents the sum of the autocorrelation matrix A along its rows. The periodicity p of the signal can then be determined based on the impulse of SA. Once the signal period is identified, the time-frequency spectral matrix is segmented into N segments, each with a length equal to period p. The shape of each segment is given by:

$$P(n) \in (k \times p) \tag{4}$$

A standard modal representation was then derived by integrating information from all N segments of the time-frequency spectrum. The standard modal representation maintains the same shape as the time-frequency spectrum of a single period, with each element determined as the median of the corresponding values across all power spectra. The standard modal is computed as follows:

$$S(i,j) = \underset{n=1,2,\ldots,N}{\text{median}} P(n)(i,j) \tag{5}$$

where, N represents the number of power spectra segmented in accordance with the period. The time-frequency spectra that the standard modal representation traverses N periods were compared to obtain the recurrence spectrogram:

$$R(i, j + (n-1)p) = \min(S(i,j), X(i, j + (n-1)p) \tag{6}$$

where, R represents the recurrence spectrogram; $i = 1, 2, \ldots, K$ is the number of rows in the standard modal representation S; $j = 1, 2, \ldots, p$ denotes the number of columns in S; and $n = 1, 2, \ldots, N$ represents one signal period.

The recurrence spectrogram R was then element-wise divided by the original time-frequency spectrum to compute the soft time-frequency mask:

$$RM(i,j) = \frac{R(i,j)}{X(i,j)} \tag{7}$$

where, RM represents the soft time-frequency mask matrix, and X denotes the original time-frequency spectrum. The soft time-frequency mask stores the relationship between the time-frequency spectrum of the signal and the standard modal representation.

A threshold selection process was applied to the soft time-frequency mask to obtain the final time-frequency mask:

$$M(i,j) = \begin{cases} 0, RM(i,j) < t \\ 1, RM(i,j) > t \end{cases} \tag{8}$$

where, M represents the final time-frequency mask matrix, and t is the predefined threshold. By multiplying the time-frequency mask with the original time-frequency spectrum, the non-stationary noise can be eliminated:

$$X1(i,j) = M(i,j) \times X(i,j) \tag{9}$$

where, $X1$ is the processed time-frequency spectrum after applying the mask. By performing an inverse transform on the processed time-frequency spectrum, the denoised background signal can be obtained. The foreground noise signal is then obtained by subtracting the background signal from the original signal:

$$x_{bp}(n) = \text{ISTFT}(X1) \tag{10}$$

$$x_{fp}(n) = x(n) - x_{bp}(n) \tag{11}$$

where, $x_{bp}(n)$ represents the background signal, and $x_{fp}(n)$ represents the foreground signal.

Figure 1 illustrates the time-frequency representation of impact noise generated by the gearbox of a hoist system. The impacts occur around 2, 3, and 4 seconds in the time-frequency spectrogram. Due to the short duration and concentrated energy distribution of the impact noise, three distinct peaks appear in the spectrogram, obscuring the time-frequency distribution of the original normal vibration signal. Figure 2 presents the time-frequency mask matrix computed by the proposed algorithm for suppressing impact noise. The mask values in the mask matrix at the three impact occurrences are observed to be close to zero, effectively filtering out the non-stationary noise in these time intervals. In contrast, the mask values at other time points remain close to one, ensuring the preservation of the original normal signal.

Figure 3 presents the time-frequency representation of the signal after denoising using the time-frequency mask noise filtering algorithm. It can be observed that the time-frequency mask algorithm effectively filters out sharp, non-stationary noise while restoring the original stationary healthy signal. As a result, interference from non-stationary noise is eliminated, reducing the likelihood of false fault detection.

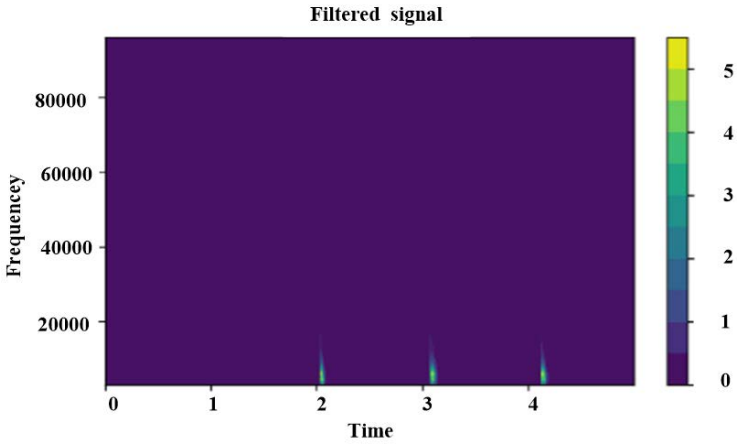

Figure 1. Impact noise

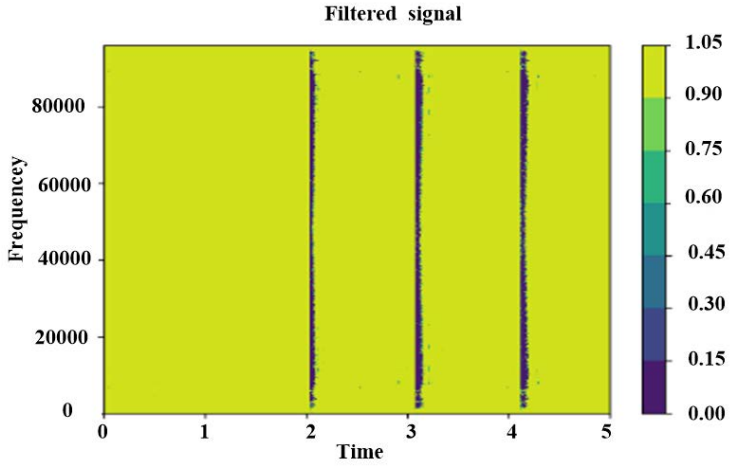

Figure 2. Time-frequency mask matrix spectrogram

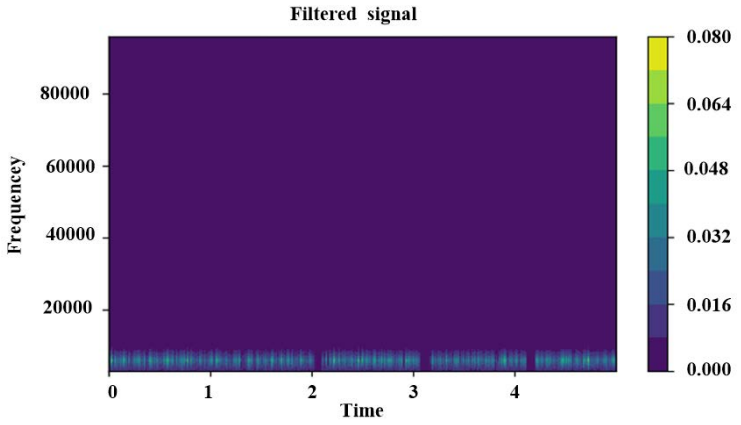

Figure 3. Time-frequency representation of the denoised signal

3 Vibration Hazard Characterization Based on Sparse Representation

Sparse representation expresses data using a dictionary and sparse coefficients:

$$Y = DX \tag{12}$$

where, $Y \in R^{N \times M}$, with N denoting the number of variables and M the number of samples; $D \in R^{N \times K}$, with K denoting the number of atoms in the dictionary, representing the dictionary capacity; $X \in R^{K \times M}$ is the sparse

coefficient. The sparse coefficient matrix contains as many zero elements as possible, ensuring that the original signal is reconstructed using the minimal number of dictionary atoms.

The solution process of the K-Singular Value Decomposition (K-SVD) is an optimization process: $\min_{D,X} \|Y - DX\|_F^2$

$$\text{s.t. } \forall i, \|x_i\|_0 \leq T_0 \tag{13}$$

where, $\|x_i\|_0$ represents the number of nonzero elements in each sparse coefficient vector. The objective of this optimization is to achieve minimal reconstruction error while preserving the sparsity constraint on the coefficient matrix.

During the offline training phase, normal sample data were collected, and an adaptive complete dictionary was learned using K-SVD. The Orthogonal Matching Pursuit (OMP) algorithm was then employed to search for atoms in the dictionary that best match the test samples and to compute the corresponding sparse vectors, enabling sample reconstruction. Kernel density estimation was applied to fit the reconstruction error of normal samples, with the 95th percentile of the reconstruction error serving as the threshold. For samples monitored online, the complete dictionary of normal samples and the OMP algorithm were used to reconstruct the online samples. The reconstruction error was computed in real time. When the error exceeds the predefined threshold, the presence of a potential hazard is inferred.

Vibration data from a normal hoister gearbox were collected as health samples, along with vibration signals representing both normal operating conditions and those containing potential hazards. Each type of sample consisted of 16 seconds of vibration data, with every 0.01-second segment from the first 0.04 seconds being used as an individual sample. As a result, 400 samples were obtained for each category, with each sample containing 1,920 data points. The data, after being denoised using the time-frequency mask technique, were utilized as the raw samples for sparse representation to evaluate the effectiveness of the hazard characterization method.

Table 1 presents the accuracy of the sparse representation algorithm in hazard characterization. A comparative analysis was conducted against classical classification algorithms, including SVM and CNN, as well as the conventional unsupervised hazard characterization algorithm, PCA. The results demonstrate that sparse representation achieves the highest accuracy among the tested methods.

Table 1. Hazard characterization results based on sparse representation

Hazard Type	SVM	CNN	PCA	Sparse Representation
Type 1	80.25%	86.75%	96.85%	97.75%
Type 2	97.85%	92.5%	95.5%	98.5%
Overall	89.05%	89.63%	96.18%	98.13%

4 Conclusion

The time-frequency mask noise filtering algorithm effectively eliminates sharp, non-stationary noise in vibration hazard signals from mining equipment, significantly reducing the likelihood of false alarms. In addition, the sparse representation algorithm outperforms SVM, CNN, and PCA in vibration hazard characterization, achieving the highest accuracy.

Data Availability

The data used to support the findings of this study are available from the corresponding author upon request.

Conflicts of Interest

The authors declare that they have no conflicts of interest.

References

[1] J. Guo, "Research on fault diagnosis method of coal machine equipment based on differential oscillator," *Coal Mine Machi.*, vol. 0, 2023.

[2] G. Yang, W. Y. Xu, Q. Deng, Y. Q. Wei, and F. Li, "Review of rolling bearing composite fault diagnosis based on vibration signal," *J. Xihua Univ.*, vol. 43, no. 1, p. 48, 2024. https://doi.org/10.12198/j.issn.1673-159X.5096

[3] G. X. Diao and Y. Y. Tang, "Study on transformer fault acoustic fingerprint diagnosis method based on masked autoencoder technology," *Noise Vibr. Control*, vol. 2023, no. 3, pp. 142–148, 2023.

[4] B. N. Wu, "Application research of vibration monitoring fault diagnosis technology in large mechanical equipment," *China High-tech.*, vol. 2023, no. 6, pp. 139–141.

[5] Y. Lu, D. Ge, Q. Gao, B. Qiao, and G. Chen, "Research on aero-engine fault diagnosis based on vibration signal," *Chinese Equi. Engi.*, 2023. http://doi.org/10.3969/j.issn.1671-0711.2023.13.076

[6] W. X. Xu, J. Zheng, and Z. D. Tian, "Intelligent algorithm-based rolling bearing fault diagnosis method under vibration excitation," *Mech. Electr. Equip.*, vol. 40, no. 5, pp. 30–34, 2023.

[7] J. Z. Wei, "Application of vibration detection technology in fan bearing fault diagnosis," *Mold Manufa.*, vol. 2023, no. 12, pp. 261–263.

[8] H. N. Cai and X. Liu, "Research and application of intelligent diagnosis method for vibrating fault of coal mining machine boom," *Coal Mine Machi.*, vol. 44, no. 11, pp. 180–182, 2023.

[9] Z. H. Li and D. J. Lu, "Research on rolling bearing fault diagnosis method based on vibration image and convolutional neural network," *Constru. Machi.*, no. 5, pp. 60–66, 2023. https://doi.org/10.3969/j.issn.1000-1212.2023.05.012

[10] B. Fu, "Mechanical fault diagnosis and recognition based on vibration image feature extraction," *Combi. Machi. Tool Autom. Tech.*, no. 3, pp. 131–135, 2021. http://doi.org/10.13462/j.cnki.mmtamt.2023.03.032

[11] D. E. Matthew, J. Shi, M. Hou, and H. Cao, "Improved STFT analysis using time-frequency masking for chatter detection in the milling process," *Measurement*, vol. 225, p. 113899, 2024. https://doi.org/10.1016/j.measurement.2023.113899

[12] G. Wojnar, R. Burdzik, N. Andrzej Wieczorek, and L. Konieczny, "Multidimensional data interpretation of vibration signals registered in different locations for system condition monitoring of a three-stage gear transmission operating under difficult conditions," *Sensors*, vol. 21, no. 23, p. 7808, 2021. https://doi.org/10.3390/s21237808

[13] I. Bagri, K. Tahiry, A. Hraiba, A. Touil, and A. Mousrij, "Vibration signal analysis for intelligent rotating machinery diagnosis and prognosis: A comprehensive systematic literature review," *Vibration*, vol. 7, no. 4, pp. 1013–1062, 2024. https://doi.org/10.3390/vibration7040054

[14] N. Andrzej Wieczorek, L. Konieczny, R. Burdzik, G. Wojnar, K. Filipowicz, and M. Kuczaj, "A complex vibration analysis of a drive system equipped with an innovative prototype of a flexible torsion clutch as an element of pre-implementation testing," *Sensors*, vol. 22, no. 6, p. 2183, 2022. https://doi.org/10.3390/s22062183

[15] A. Althubaiti, F. Elasha, and J. A. Teixeira, "Fault diagnosis and health management of bearings in rotating equipment based on vibration analysis–A review," *J. Vibroeng.*, vol. 24, no. 1, pp. 46–74, 2022. https://doi.org/10.21595/jve.2021.22100

[16] M. R. Bhuiyan and J. Uddin, "Deep transfer learning models for industrial fault diagnosis using vibration and acoustic sensors data: A review," *Vibration*, vol. 6, no. 1, pp. 218–238, 2023. https://doi.org/10.3390/vibration6010014

[17] L. Brezzi, F. Gabrieli, D. Vallisari, E. Carraro, A. Pol, A. Galgaro, and S. Cola, "Diphorm: An innovative digital PHOtogrammetRic monitoring technique for detecting surficial displacements of landslides," *Remote Sens.*, vol. 16, p. 3199, 2024. https://doi.org/10.3390/rs16173199

[18] Z. Chen, A. Mauricio, W. Li, and K. Gryllias, "A deep learning method for bearing fault diagnosis based on cyclic spectral coherence and convolutional neural networks," *Mecha. Syst. Signal Process.*, vol. 140, p. 106683, 2020. https://doi.org/10.1016/j.ymssp.2020.106683

[19] M. J. Hasan, A. Rai, Z. Ahmad, and J. M. Kim, "A fault diagnosis framework for centrifugal pumps by scalogram-based imaging and deep learning," *IEEE Access*, vol. 9, pp. 58 052–58 066, 2021. https://doi.org/10.1109/access.2021.3072854

[20] E. C. Ozkat, "Vibration data-driven anomaly detection in uavs: A deep learning approach," *Engi. Sci. Tech. Int. J.*, vol. 54, p. 101702, 2024. https://doi.org/10.1016/j.jestch.2024.101702

[21] H. Mostafaei, "Modal identification techniques for concrete dams: A comprehensive review and application," *Sci*, vol. 6, no. 3, p. 40, 2024. https://doi.org/10.3390/sci6030040

[22] K. Vos, Z. Peng, C. Jenkins, M. R. Shahriar, P. Borghesani, and W. Wang, "Vibration-based anomaly detection using LSTM/SVM approaches," *Mech. Syst. Signal Proc.*, vol. 169, p. 108752, 2022. https://doi.org/10.1016/j.ymssp.2021.108752